Microchemical Journal 119 (2015) 114–122

Contents lists available at ScienceDirect

Microchemical Journal

journal homepage: www.elsevier.com/locate/microc

SR μXRF and XRD study of the spatial distribution and mineralogical composition of Pb and Sb species in weathering crust of corroded bullets of hunting fields

María F. Mera [a], Marcelo Rubio [a,b,c,*], Carlos A. Pérez [d], Víctor Galván [b,c], Alejandro Germanier [a]

[a] CEPROCOR, Álvarez de Arenales 230, B° Juniors, 5000 Córdoba, Argentina
[b] Facultad de Matemática, Astronomía y Física (FAMAF), Ciudad Universitaria, M. Allende y H. de la Torre, Córdoba, Argentina
[c] CONICET, Rivadavia 1917, 1033 Buenos Aires, Argentina
[d] LNLS, Laboratorio Nacional de Luz Sincrotron, Rua Giuseppe Máximo Scolfaro, 10000, Guará, Campinas, SP 13083-100, Brazil

ARTICLE INFO

Article history:
Received 22 November 2014
Accepted 26 November 2014
Available online 3 December 2014

Keywords:
Micro X-ray fluorescence
Synchrotron
X-ray diffraction
Lead
Antimony

ABSTRACT

The spatial distribution of Pb and Sb in core and crust material and the mineralogical composition of these elements in weathering crust of corroded bullets found in hunting fields were investigated. Lead, antimony and others metals from pellets alloy are disperse in the soil of the shooting fields. As long as the corroding bullets are present in soil, secondary Pb and Sb phases appear in the weathering crusts being an important source of bioavailable Pb and Sb.

Powder X-ray diffraction (XRD) patterns of crust material from weathered bullets showed encrustation of relevant Pb and Sb phases like: hydrocerussite ($Pb_3(CO_3)_2(OH)_2$), litharge (PbO-tetragonal), hydroxypyromorphite ($Pb_5(PO_4)_3(OH)$), gebhardite ($Pb_8OCl_6(As_2O_5)_2$, Sb metallic, stibnite (Sb_2S_3), tripuhyite ($FeSbO_4$) and potassium sodium antimony oxide ($KO_{13}Sb_5$) among others minor compounds.

The chemical elemental distribution of corroded bullets was determined by synchrotron radiation-induced micro X-ray fluorescence analysis (SR-μXRF). A positive correlation between Sb and Fe was detected in crust material measured in the outer rim of the weathered bullets due to Sb adsorption to Fe oxyhydroxides of soil. It was also observed a spatial correlation between Sb and Cu and between Sb and Zn in crust. The influence of phosphorus applied as (P)-based fertilizers of soils was observed in the hydroxypyromorphite phase detected in samples collected near agricultural lands.

1. Introduction

The aim of this work is to study the spatial distribution of Pb and Sb and to determine the mineralogical composition of these elements on core and crust material from weathered bullets. Hunters release Pb and other metals in shooting sites from the use of newly manufactured ammunitions and shots. This represents a potential source for toxic metals contamination in soils [1–7]. Bullets are mainly composed of Pb (90–95%), Sb (2–4%), Cu and other metallic traces, which are added to harden the alloy, prevent deformation and maintain aerodynamic stability [2].

Once bullets and its fragments are deposited on soil, the metallic cores begin an oxidation process controlled by chemical reactions with the soil components. Consequently, Pb and Sb mineral phases grow in the surface of the bullets. Most investigations about contamination of spent bullets are focused on the release of Pb to environment, and are lower than those who try about release of Sb or other metals. PbO is the first compound resulting from the direct oxidation of metallic lead by oxygen. Massicot and litharge are both mineral phases of PbO, but massicot is reported as a metastable phase found that litharge is the first weathering product. In the presence of CO_2 litharge is transformed in hydrocerussite [10].

Although researches on the corrosion mechanism of Sb from bullets are only few, studies of quantitative Sb speciation in shooting ranges are increasing. The environmental toxicity of Sb compounds is understood similar to As. Experiences in walled shooting ranges show that Sb mostly is present as anoxidized bullet core grains. Sb is present as elemental Sb grains, but it was also found in Fe- and Pb-rich crusts around soil particles and in Fe- and Pb-rich individual conglomeratic grains. Grains of crust are released from weathering bullets giving rise to contaminant toxic metals of top and subsoils [9–12]. For instance, it was shown that Sb forms inner-sphere complexes with Fe oxide soil phases, as well as binds to soil organic matter such as humic acid [3]. Soil humic acid is an important part of the soil organic matter that facilitates the transport of several arrays of inorganic and organic contaminants [13,14].

* Corresponding author at: CEPROCOR, Álvarez de Arenales 230 B° Juniors, 5000 Córdoba, Argentina. Tel.: +54 3541 489651/53; fax: +54 3541 488181.
E-mail address: mrubiocba@yahoo.com (M. Rubio).

http://dx.doi.org/10.1016/j.microc.2014.11.010
0026-265X/

Nevertheless, the mechanism by which Sb is bind to Fe oxides and humic acids is still not completely understood.

In this work, six Pb and four Sb major crystallographic mineral compounds were quantified in crust from those identified by X-ray diffraction experiments. Mapping of chemical elements taken by SR-μXRF on cross section of halved weathered bullets showed that Sb in the border of core is mostly accumulated in those regions where there is also high concentration of Fe, Cu or Zn. Micro scanning of Pb in crust shows a positive spatial correlation between Pb and Fe.

2. Materials and methods

2.1. Geography of the site

The center-north region of the Province of Córdoba, Argentina (geographical region limited between parallels S31 and S30 and between meridians W64 and W63) is a worldwide recognized tourist region for dove hunting. The region studied is shown into the map of Córdoba in Fig. 1 (area bounded by the black edges of the rectangle). Its limits are the parallels S30 04.771 and S31 21.897 and the meridians W64 17.315 and W63 00.00. It was adopted the World Geodetic System 84 protocol to show the GPS coordinates in degrees, minutes, and thousandths of minutes for latitude (S) or longitude (W). The native forest of the region has a great population of doves associated with surrounding grain production fields. Hunting sites are located at open natural fields (they are not walled shooting ranges which represent sites that are heavily polluted) authorized by the environmental authorities applying national and local norms to regulate the hunting activities as well as the prevention of soil pollution.

Sample collection was taken on the north-west side and east side of the studied region. The north-west geomorphology reaches 650 m of altitude and is crossed by the hill called “Sierra Norte” that belongs to the Sierras Pampeanas orographic system. This mountain chain crosses the province of Córdoba from north to south and is composed by granitic, metamorphic, and sedimentary rocks. The soil is classified as calcic to petrocalcic. The geomorphology of the soil of the eastern hunting region is ‘Flat pampa’ type: up to 150 m of altitude with plain relief, slow runoff with well drainage. The biota consists of grasses and crops. The soil can be classified as Argiustol, typic from the family of fine limo. No samples were taken in the region situated in the surrounding of the ‘Anzenuza’ lake because no sport hunting activities are allowed there.

2.2. Samples

2.2.1. Soil samples

Soils samples were collected in 36 hunting fields of the studied region, described in details by the authors in a previous work [8]. At each firing zone, 10 GPS referenced points symmetrically distributed in a 100 × 100m^2 square sector of ground were chosen to collect soil material (nine points equally distributed in the square perimeter and

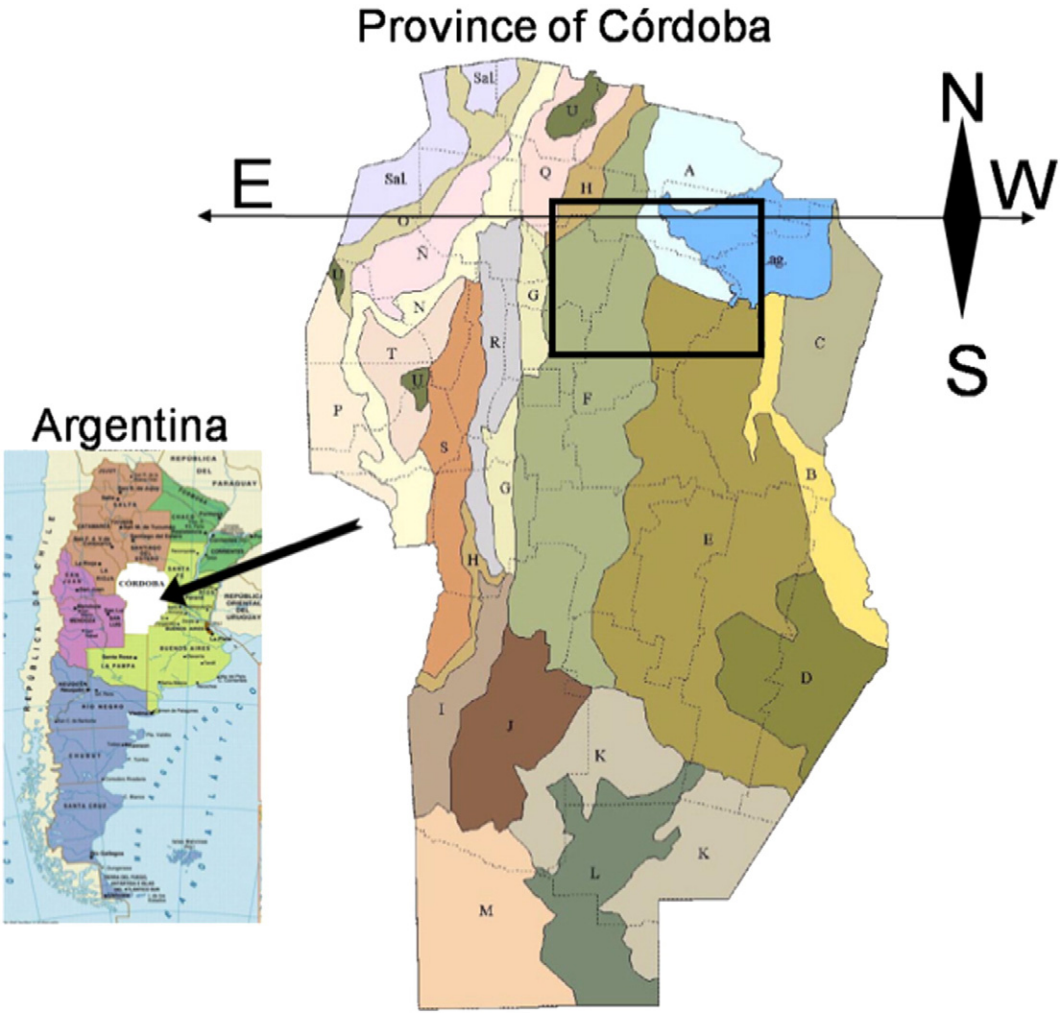

Fig. 1. Relative location of the province of Cordoba into the map of Argentina (left). The studied region is shown as a rectangle located in an area limited by the parallels S30 04.771 and S31 21.897 and the meridians W64 17.315 and W63 00.00.

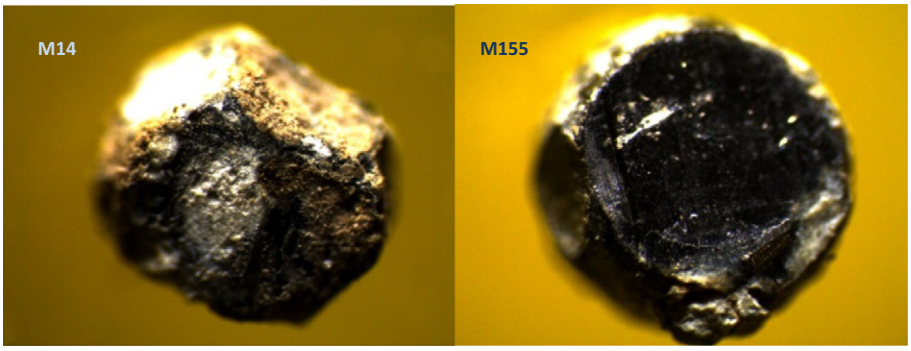

Fig. 2. Motic optical microscope (40 ×) images of samples M14 and M155 of weathered bullets mounted on a kapton adhesive surface. SR μ-XRF linear scanning was done in zones of those visible faces.

one in the center). The samples at the perimeter were collected at 50 mm depth, whereas the ones at the central points were taken at 5 and 15 cm depth.

2.2.2. Weathered bullets samples

Weathered bullets were collected in the laboratory within the same process to provide the soil for pressed pellets samples for XRF analysis. An aliquot of 80 g of each soil sample collected was dried in oven at 60 °C for 24 h to remove water and volatile compounds. After cooling at room temperature, the soil was smoothly grounded using a porcelain mortar in order to reduce the granulometry of larger clods. Then, the soil material was sieved in a 200-mesh plastic sieve (74 μm). The bullets retained in the sieved process were separated, cleaned of external dust and classified. Analyses of the collected spent pellets have been shown to be visibly corroded and covered with a crust of white, gray or brown material [8].

2.2.3. Crust samples

The crust material was prepared by blending crust powder obtained from groups of approximately 15 weathered bullets. A time-controlled mixer was used to shake each group of bullets. After several tests we determine that a shaking time of 15 s is the best option to maximize the quality of the crust power. Higher mixing times may alter the crystals, whereas lower times are not enough to ensure homogeneity. After mixing the powder was separated from the cores of bullets. Crust powder was prepared separately for bullets collected in the north and in the east hunting region, because the composition of the corresponding topsoils is slightly different. Crust powder was placed and compacted in two holes on an acrylic sample holder for SR micro-XRF experiences. Also, it was mounted on a Si holder of low background for XRD experiences.

2.3. Analytical techniques

2.3.1. X-ray fluorescence

Conventional fluorescence analysis of soil samples was performed at CEPROCOR using a 4 kW power Bruker SRS 3400 wavelength dispersive spectrometer [8].

Weathered bullets were analyzed by SR-μXRF. The bulk elemental composition of bullets was determined at a standard geometry (45–45°) using a silicon drift detector (KETEK GmbH) with a resolution of 140 eV (FWHM) at 5.9 keV. Measurements were performed in normal conditions of temperature and pressure.

The composition of the coatings was determined by a) a μXRF linear scan of 8 pixels on the outer surface of selected corroded bullets with a counting live-time of 20 s in pixels spaced 200 μm from each other and b) by irradiating the crust powder samples.

Three selected bullets were prepared in halves of spheres and fixed in contaminant-free epoxy resin with its polished flat face oriented to the synchrotron white beam for excitation. The surfaces of samples were irradiated in order to carry out elemental mappings. SR-μXRF 2D maps were performed on areas covering representative parts of the bullets (almost 100% of the total sample cross section). An X-ray optic based on the use of a pair of dynamically figured mirrors in a so-called KB mirror arrangement was used. The microfocusing system, fabricated by the X-ray optic group [15] of the European Synchrotron Radiation Facility (ESRF) in France, is able to produce an X-ray microbeam of around 12 μm × 20 μm in size. A selenium (Se) filter was used in order to reduce distortion of the XRF spectra due to the high X-ray fluorescence intensity contribution of the Pb-L lines mainly coming from the core of the bullet. Samples were put in the focus plane within an accuracy of 1 micron with precise remote-controlled motorized stages. An optical microscope (magnification of 500×) was used to visualize the sample and to precisely reference the irradiated pixels. Scan steps of 30 μm and 20 μm were selected to perform XRF maps on the

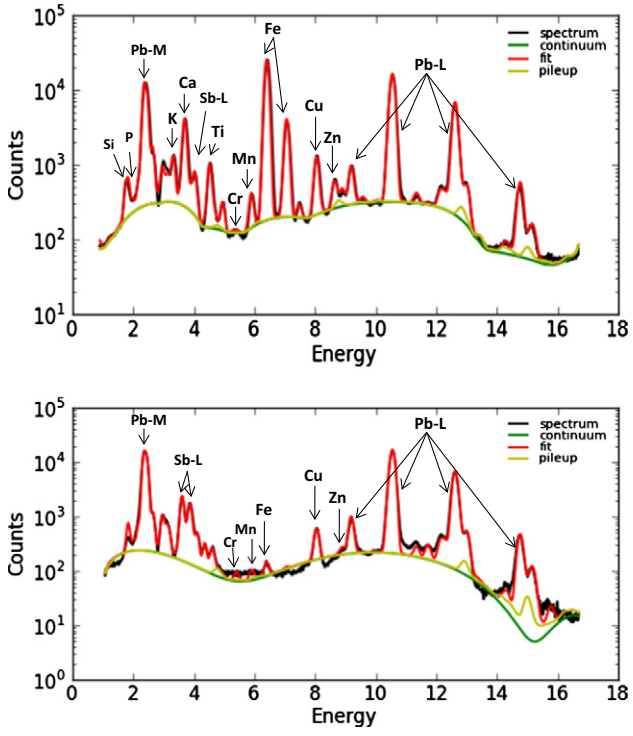

Fig. 3. Representative XRF spectra induced by synchrotron radiation taken in pixels of 20 × 20 μm during 20 s in surfaces of bullets samples M14 (up) and M155 (down).

Table 1
Synchrotron radiation μXRF quantitative elemental analysis and conventional XRD mineral speciation associated in crust samples.

Z	Composition of crust in powder		Composition of crust in bullet	Mineral phases of crust		DRX quantitative analysis	
	East zone	West–North zone	ppm *or* %	Chemical formula	Compound name	East zone %	West–North zone %
Na	NA[a]	NA	NA	$(Na_{0.75}\ Ca_{0.25})\ Al_{1.2}6\ Si_{2.74}\ O_8$	Plagioclase	9.3	2.5
Al	NA	NA	NA	$(Na_{0.75}\ Ca_{0.25})\ Al_{1.2}6\ Si_{2.74}\ O_8$	Plagioclase	9.3	2.5
Si	1.30%	0.88%	12%	$(Na_{0.75}\ Ca_{0.25})\ Al_{1.2}6\ Si_{2.74}\ O_8$	Plagioclase	9.3	2.5
				SiO_2	Quartz	28.2	28.6
				$Pb(Ca, Mn)_2\ (SiO_3)_3$	Margarosanite	0.5	0.3
P[b]	0.77%	1.40%	11%	$Pb_5(PO_4)3(OH)$	Hydroxypyromorphite	5.4	3.4
Cl	0.73%	0.81%	1.75%	$Pb_8OCl_6\ (As_2O_5)_2$	Gebhardite	4.5	2.4
K	0.31%	494 ppm	0.60%	$KO_{13}Sb_5$	Potassium sodium antimony oxide	2.2	1.1
Ca	0.80%	0.23%	1.40%	$Pb(Ca,Mn)_2(SiO_3)_3$	Margarosanite	0.5	0.3
				$Na_{0.75}\ Ca_{0.25})Al_{1.2}6\ Si_{2.74}\ O_8$	Plagioclase	9.3	2.5
Ti	0.20%	633 ppm	0.22%				
V	84 ppm	27 ppm	84 ppm				
Cr	22 ppm	20 ppm	4 ppm				
Mn	264 ppm	95 ppm	236 ppm	$Pb(Ca,Mn)_2(SiO_3)_3$	Margarosanite	0.5	0.3
Fe	0.92%	0.70%	1.70%	$FeSbO_4$	Tripuhyite	0.2	1.4
Ni	3 ppm	8 ppm	55 ppm				
Cu	288 ppm	478 ppm	627 ppm				
Zn	54 ppm	58 ppm	220 ppm				
Sb	0.60%	0.80%	0.40%	Sb_2S_3	Stibnite	1.6	3.5
				Sb_2O_4	Antimony oxide	1	1
				Sb	Antimony	0.7	0.5
				$FeSbO_4$	Tripuhyite	0.2	1.4
				$KO_{13}Sb_5$	Potassium sodium antimony oxide	2.2	1.1
Pb	41%	49%	50%	Pb	Lead	1.0	1.3
				$Pb_3\ (CO_3)_2\ (OH)_2$	Hydrocerussite	38.2	37.5
				PbO (tetragonal)	Litharge	1.6	10.5
				PbO (ortorrómbico)	Massicot	< LD[c]	< LD
				$Pb(SO_3)$	Lead sulfate	1.1	2.5
				PbS	Lead sulfide	0.4	0.3
				$Pb(Ca, Mn)_2(SiO_3)_3$	Margarosanite	0.5	0.3
				$Pb_5(PO_4)3(OH)$	Hydroxypyromorphite	5.4	3.4
				$Pb_8OCl_6(As_2O_5)_2$	Gebhardite	4.5	2.4
				Pb_2OCO_3	Shannonite	4.2	3.3

[a] NA: element not analyzed.
[b] Relative uncertainty of phosphorus was 55% due to hard overlapping with Pb–M series.
[c] Less than the limit of detection.

whole area of the halved bullets surfaces. Spectra were processed using the PyMca software [16], an advanced fitting program developed by the ESRF.

All experiments with SR were carried out at the D09B XRF Fluorescence beamline of Brazilian Synchrotron Radiation Laboratory (LNLS) in Campinas, Brazil [17].

2.3.2. X-ray diffraction

Diffraction patterns of corroded crust samples were collected with a PANalytical-Empyrean diffractometer with Cu-Kα X-rays, a post-diffraction graphite monochromator, at 40 kV 40 mA, step size 2θ of 0.02°. The counting time was 400 s per step, using the area detector PIXcel[3d]. In all cases, since too small amounts (a few milligrams) of material were available, samples were mounted on a Si holder of low background. The sample holder was axially rotated a speed of 30 rpm to reduce preferred orientation effects.

The crystalline phases present were quantified by Rietveld refinement, as implemented in the DiffracPlus TOPAS® commercial software. (Bruker-AXS, Germany)

2.3.3. Rietveld refinement

The Rietveld refinement method uses a least squares approach to refine a theoretical XRD spectrum until it matches the measured profile [18]. The model for the calculated profile includes structural (spatial groups, atoms in the asymmetric units, thermic factors, etc.), microstructural (concentration, crystal size, micro deformations), and instrumental (full width at half maximum, width of slits, size of the sample, depth of X-ray penetration, etc.) factors.

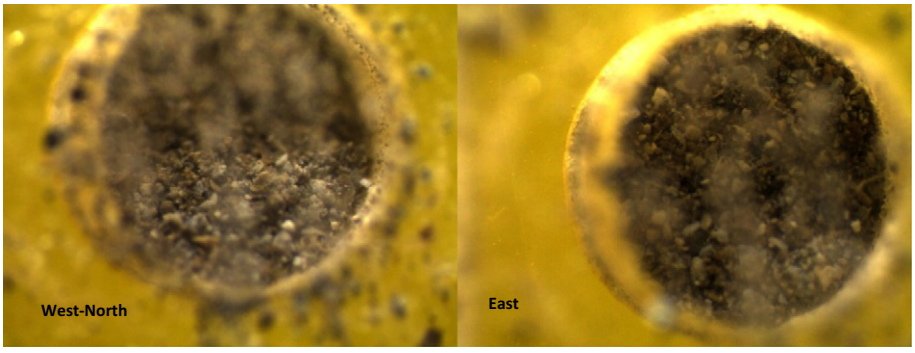

Fig. 4. Crust powder samples for SR-XRF analysis. The material extracted from groups of corroded bullets of west-north region (left) and east region (right) was compacted in holes made on an acrylic sample holder.

A Pearson VII profile function [19] was used in this work for approximating the X-ray diffraction peaks; this model, based on a Gaussian function multiplied by a correction factor in the form of a series expansion in Hermite polynomials, was chosen since it takes into account the asymmetry of the peaks. The preferred orientation effects were corrected for the easily orientable phases (e.g. feldspars). The background was fitted using a sixth degree polynomial function. Parameters related to thermal fluctuations were not refined, since their influence will be negligible as compared to the uncertainties introduced by the refinement of occupancy factors, in view of the poor statistics associated to the minor phases. The values for these parameters were taken from the Inorganic Crystal Structure Database (ICSD) indexed files corresponding to each mineral.

In order to provide a figure of merit for the performance of each fit, the goodness of fit is assessed through the weighted comparison of the predicted intensities $\tilde{Y}i$ with the experimental ones Yi:

$$GOF = \sqrt{\frac{1}{N-P_i}\sum_{i=1}^{N}\frac{\left(Y_i-\tilde{Y}\right)^2}{Y_i}}$$

where i denotes each of the N channels in the considered XRD spectrum, and P is the number of free parameters in the fitting process. The statistical quality of the fit is represented through the *Re* parameter, defined as

$$R_e = \sqrt{\frac{N-P}{\sum Y_i}}$$

3. Results and discussion

3.1. XRF analysis of soil

In a previous work [8] the authors investigated the Pb contamination in soils of shooting fields located in the hunting zone. The multielemental quantitative XRF analysis performed in 315 dried and sieved soil samples reported an average concentration of 80 ppm for lead. Antimony was not quantified because it is below the XRF quantification limit due to several causes like: a) uncontaminated soils of the region have traces level of Sb, b) Sb is a minority element in the bullets alloys and c) hard overlapping between Ca Kα fluorescence line and Sb Lα,β lines.

Hunting soils are rich in Fe oxides whose origins are the mineral composition of parent silicate rocks (predominant in the west-north region studied) as well as Fe-oxides aggregates in the east.

3.2. SR μXRF elemental analysis of bullets

Bulk elemental composition of corroded ammunitions commonly used in Argentina was determined by SR μXRF. Samples M14 and M155 shown in Fig. 2 are bullets in the process of weathering when being collected and were selected for elemental crust quantification. Fig. 3 shows the corresponding X-ray fluorescence spectra taking by irradiation of the surface of the bullets in pixels of 20 μm × 20 μm during 20 s. The upper spectrum corresponds to sample M14 and it is dominated by Pb-L series and Fe Kα lines and Sb is identified and fitted even the interference of Ca. This spectrum is equivalent to each of the other spectra taken in a scan transect of 8 pixels. The average concentrations for major elements measured in M14 are shown in the 4th column of Table 1. It can be observed that the composition of Fe is 1.7%. The lower graph of Fig. 3 shows a representative spectrum of sample M155 in the inner zone (core of the bullet with a less corrosion process than in the border). It can clearly be seen that the iron does not dominate the distribution of elements. The average composition in this zone is Pb 57%; Sb 2%; Cu 270 ppm; Fe 28 ppm; Cr 15 ppm; Zn 3 ppm; and Mn 4 ppm. The analytical comparison between M155 and M14 indicates a decrease in the concentration of Pb and Sb and growing concentrations of Fe, Cu and Zn, being a concrete evidence of the progress of corrosion.

It can be observed the important decreasing in the concentration of Pb between core of pristine bullets (~ 90–95%), Pb concentration in core of bullets with minor corrosion process (~ 57%), Pb in corroded crust (~ 40–50%) and the average concentration of Pb in bulk soil of the studied region (80 ppm).

The elemental composition of crust powder was determined by SR μXRF analysis. Samples of crust powder are shown in Fig. 4 from

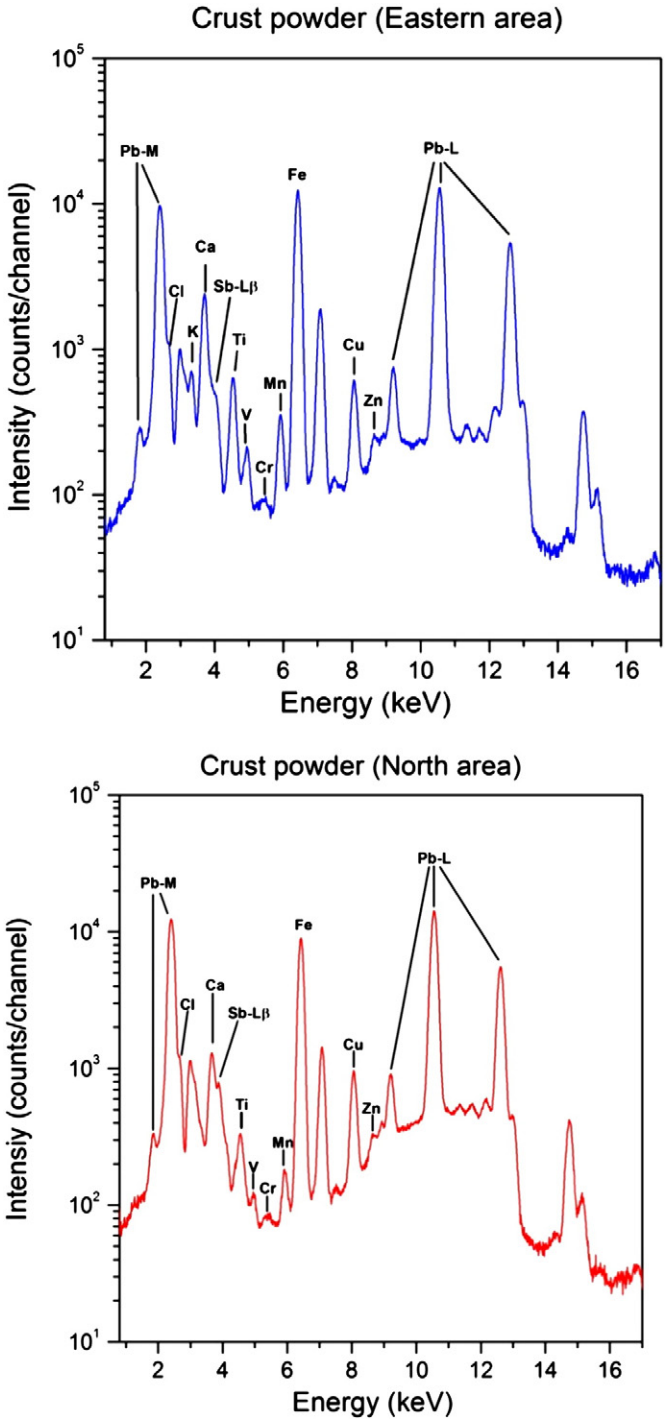

Fig. 5. Synchrotron radiation μXRF spectra of crust powder samples of east region (up) and west-north region (down).

Table 2
Chemical composition of the standards used for quantification procedures by SR-μXRF.

Elements	Pb96/Sb4 (%)	BCS-CRM 178/2 (%) [a]
Sn	–	65.76
Sb	4	7.56
Cu	–	3.664
Pb	96	2.54
As	–	0.12
Bi	–	0.088
Cd	–	0.112
Fe	–	0.019
Ni	–	0.136
Zn	–	0.032

[a] Final concentration values considering 20% dilution in wax (Merck).

material of the west-north (left) and from the east region (right). Two representative XRF spectra are shown in Fig. 5 for samples of both hunting region. The second and third columns of Table 1 show the elemental composition results of crust in powder for each region. Antimonial lead foil (Pb96/Sb 4) from Goodfellow with 0.1 mm thickness and tin base white metal (BCS-CRM 178/2) from British Chemical Standard were used as standards for the quantitative procedure (see Table 2). These analytical results are statistically significant of all crust because the irradiated material is very representative of the bullets of the whole studied region, as was described in the sample preparation section.

The composition of the crust is rich in Pb followed by Sb, Fe, Ti, Cu, Mn and Zn with traces of V, Ni and Cr. Analogous analytical results were obtained from measurements on crust on both types of samples (powder separated and adhered to corroded bullets). The presence of Fe, Ti, Cu, and Mn comes from the composition of the soil [8], while the high presence of lead and antimony is due to the composition of bullets. Cooper is also present in the alloy of core as is shown in the elemental mapping of bullets. Margarosanite is the mineral compound of Pb and Mn and was detected by XRD. The elements Na and Al were not analyzed due to the strong attenuation of their K-lines in air as well as on the beryllium window of the detector.

3.3. SR μXRF elemental mapping of bullets

SR-μXRF mapping of three selected weathered bullets named M3, M4 and M6 was performed at the X-ray microprobe station of the LNLS D09B XRF Fluorescence beamline. Typical microscale images of elemental distribution are shown in Figs. 6 to 8. Fig. 6 shows a microphotograph (left) and the corresponding μ-XRF elemental map (right) of the sample M6. A white grain highly rich in Pb (probably a hydrocerussite mineral phase) that has grown over the core can be clearly seen. A weak positive spatial correlation between Pb and Fe is visible on the core border. A result in this direction was published by Vantelon [11] who explains that the crust is formed by oxidation of metallic Pb and Sb and incorporation of elements provided by the surrounding soil or eventually the jacket of the bullets, more precisely, by the high sorption affinity of Pb to Fe oxides present in the soil matrix. The homogeneity of the Pb–Sb alloy matrix is observed in the center-right of the core as a light blue zone on the right image. No observable evidence of the presence of interlayer or mantle covering the core was detected in the bullets used in the region. Probably the manufacture only includes a carbon surface treatment on the Pb–Sb core that may replace such coating.

A microphotograph and an elemental map of sample M4 are shown in Fig. 7. The yellow spots on the Fe–Sb–Pb correlation map show that Sb is well associated with Fe in crust. This is in agreement with results obtained by other author [1] and suggests that an important fraction of Sb is associated to Fe and possibly to other minerals. A weak positive correlation between Fe and Pb is observed on the right corner (see the upper zoom image). The correlation between Zn, Sb and Pb and between Cu, Sb and Pb distribution inside the core and in the weathering crust around the bullet core are also shown in the Fig. 7. Yellow spots show that Sb in crust is well associated with Zn and Cu. White spots show the important presence of Cu in the core.

A microphotograph and a μXRF elemental map of sample M3 are shown in Fig. 8. Two zoom images labeled as a) and b) show formations of a phase rich in Pb (probably hydrocerussite) on an iron environment. Comparing with other cores studied in this work, a more uniform distribution of Pb and Sb is observed in this core, probably due to the manufacture of the alloy rather than the aging time. A positive correlation between the distribution of Pb and Fe in the crust around the core (indicated by arrows) is observed on the left rim of the bullet shown in the image c). No correlation in clearly visible between Sb and Fe.

3.4. Powder X-ray diffraction of crust

Fig. 9 shows the XRD patterns for the crust removed from bullets of the west-north and the east of the studied region. In the Rietveld

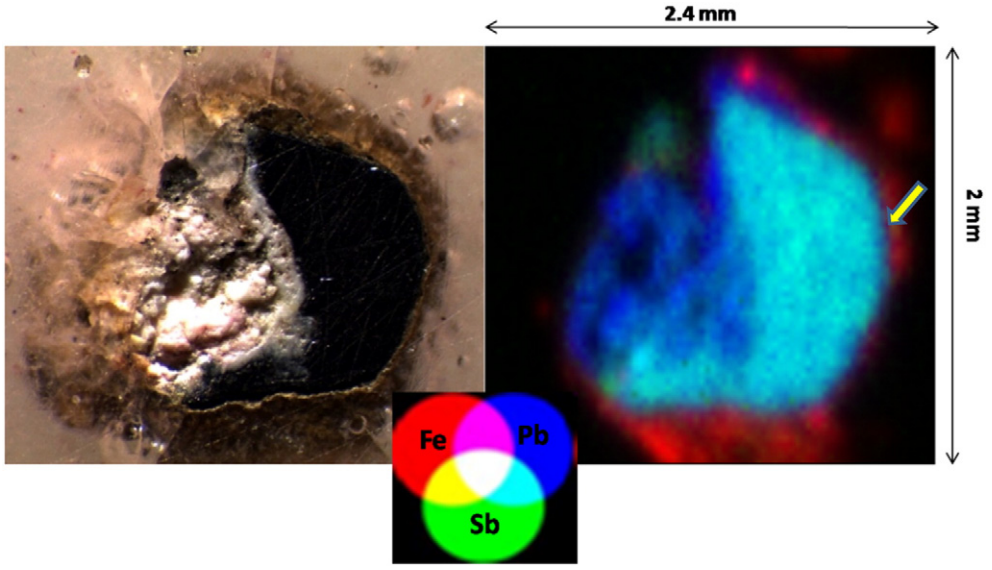

Fig. 6. Left: optical image corresponding to the M6 sample showing a hydrocerussite grain grown over the metal core. Right: SR-μXRF elemental map showing a positive spatial correlation between Pb and Fe over the right rim of the core (arrowed). Light-blue pixels inside the core represent the homogeneity of the Pb–Sb alloy.

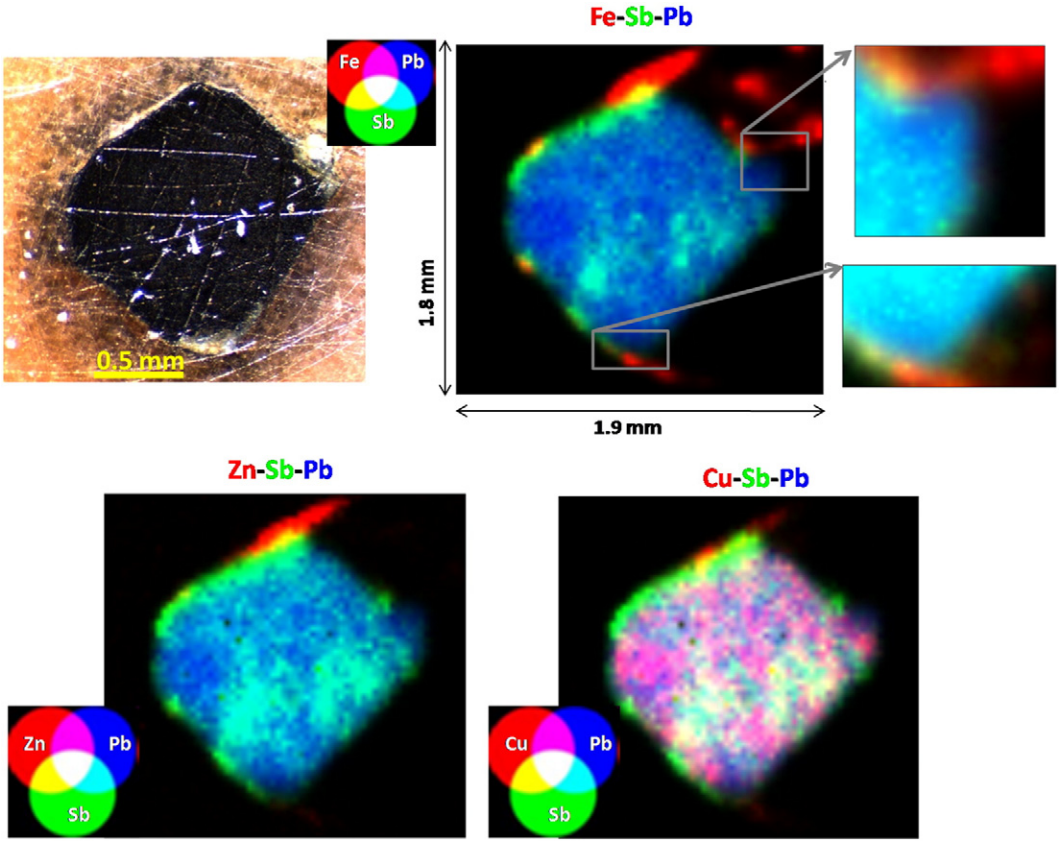

Fig. 7. Optical image and SR-μXRF elemental map of the sample M4 showing the positive correlations Pb–Sb–Fe; Zn–Sb–Pb and Cu–Sb–Pb.

refinement procedure, for some reflections, the major phase peaks are overlapped with the principal lines of minor phases, hindering the deconvolution process. Therefore, the LOD for these phases is increased. The R factors [20] (numerical criteria of fit) obtained from the refinement results are similar for both samples, $R_e = 2.5$, Rwp = 4.6 and GOF = 1.8. The apparently high values for Rwp evidence the difficulties mentioned above. Nevertheless, although the values obtained for Rwp seem to be too large, it must be pointed out that since a rather small amount of material is to be analyzed, statistics of minor phases cannot be noticeably improved due to the unavoidable experimental limitations this implies.

As can be observed in Table 1 as well as in the Fig. 9, hydrocerussite ($Pb_3(CO_3)_2(OH)_2$) is the predominant mineral of the several Pb compounds identified for both geographic regions. Hydroxypyromorphite ($Pb_5(PO_4)3(OH)$), gebhardite $Pb_8OCl_6(As_2O_5)_2$, shannonite (Pb_2OCO_3) and litharge (PbO-tetragonal) follow the majoritarian presence of hydrocerussite in the eastern region. On the contrary, in the west-north zone the order was litharge, hydroxypyromorphite, shannonite and gebhardite. Massicot was not identified. This can confirm that litharge is more stable than massicot being the first weathering product occurring in the crust. In the presence of CO_2, litharge is transformed to hydrocerussite the predominant mineral found in this work. The

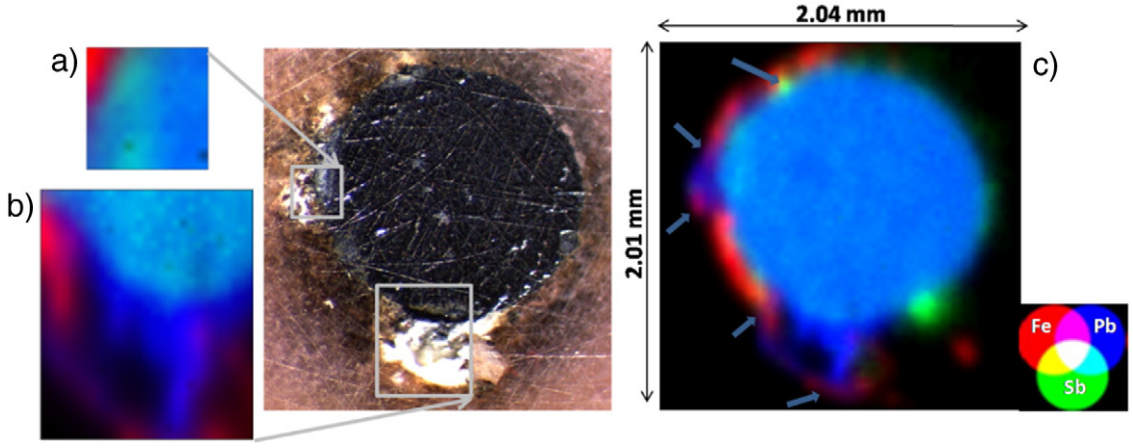

Fig. 8. Optical image and SR-μXRF elemental map of the sample M3. Two zoom images labeled as a) and b) show formations of hydrocerussite on an iron environment. The μXRF mapping on the right side c) shows a more uniform distribution of Pb and Sb in the alloy and a good positive correlation between Pb and Fe distribution in the crust over the left rim of the core (arrowed).

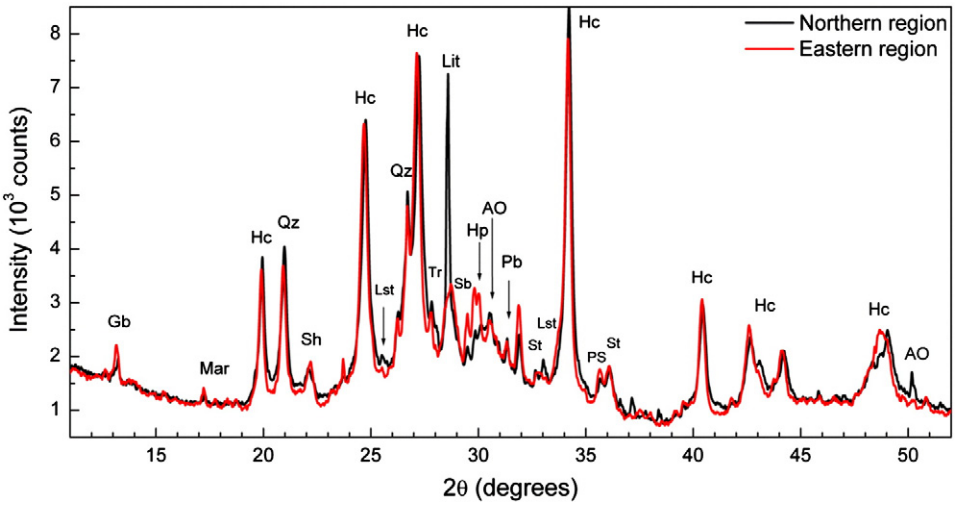

Fig. 9. XRD patterns for the crust removed from bullets of the west-north and east regions. Pb: lead, HC, hydrocerussite, Lit: litharge, Qz: quartz, Lst: lead sulfate, Lsd: lead sulfide, Mar: margarosanite, Hp: hydroxypyromorphite, Gb: gebhardite, Sh: shanonite, AO: antimony oxide, St: stibnite, Sb: antimony and Tr: tripuhyite.

presence of lead and lead sulfate was also quantified in the crust for both regions.

Hydroxypyromorphite and gebhardite are mineral phases of Pb with phosphorous and arsenic respectively. A remarkable result (see Table 1) is the higher concentration of these compounds for the eastern samples than the ones corresponding to the northern. This result can be explained by the dynamics of P and As in soil solution. Regarding phosphorous, the contribution of phosphate ions in soil comes from native inorganic P, organic P, biota P and phosphate (P)-based fertilizers applied in the agricultural land. In particular, the shooting sectors in the east region are located on the borders between "islands" of remnant native vegetation placed in a "sea" of cultivated lands. Regarding As, it is a natural contaminant of many underground aquifers and waterways of Argentina, in particular in the east of the Province of Córdoba. Underground water in the hunting region on the east can contain up to 20 times the As concentration values than the northern studied region.

Four antimony mineral compounds were identified and quantified (see Table 1). Stibnite (Sb_2S_3) followed by tripuhyite ($FeSbO_4$), potassium sodium antimony oxide ($KO_{13}Sb_5$) and antimony oxide (Sb_2O_4) are preponderant in the northern samples. But, in the eastern the concentration of $KO_{13}Sb_5$ is twice the concentration values than the northern samples. On the other hand, plagioclase and quartz are detected as soil contamination of crust (they are not mineral phases of weathered pellets). Metallic antimony was identified in samples of crust from both hunting regions.

4. Conclusions

The crust of weathering bullets used for hunting in the native forest of the Province of Córdoba, Argentina, was studied by synchrotron radiation μXRF and XRD. The bullets collected from soil samples contain high concentrations of Pb–Sb based alloy matrix with important traces of Cu. The crust composition is headed by Pb, Fe, and Sb as major metallic elements; Cu, Ti and Mn as metallic traces and other minor metallic traces like Zn, V and Cr. The XRD allowed us to detect the following Pb and Sb mineral compounds in crust (in descending order of predominance): hydrocerussite, hydroxypyromorphite, gebhardite, shannonite, litharge, stibnite, potassium sodium antimony oxide, tripuhyite, antimony oxide, and margarosanite. Some alterations in the order of predominance occur among the samples of the west-north and the east region as is shown in Table 1.

An important result of this work is the clear influence of phosphorus applied as (P)-based fertilizers of soils in the hydroxypyromorphite compound grown on crust samples of bullets collected in the east region. This mineral phase of lead is greater in eastern crust powder than in the northern samples. The presence of gebhardite is also greater in the east than in the north, probably due to the chronic incidence of higher concentrations of As in underground aquifers and waterways. We did not confirm the presence of Massicot (orthorombic PbO) in both regions, which is in coincidence with other work that studied secondary Pb mineral species in the weathering crust of shooting range soils.

The spatial distribution experiences performed by SR-μXRF determined a positive correlation between Pb and Fe in crust around cores of bullets. This is due to the high sorption affinity of Pb to Fe oxides present in rock parents as well as in iron organic compounds of our soil matrix. A significant positive correlation between Sb and Fe was detected in crust samples due to Sb adsorption to Fe oxyhydroxides. In addition, we observed a positive correlation between Sb and Cu and between Sb and Zn in crust samples. This work confirms specific literature that explains how Fe oxides act as important sinks for Sb. But, not so much is said in other works about similar results of Cu, Zn and Sb correlations.

Acknowledgments

This work was partially supported by the LNLS, National Synchrotron Light Laboratory, Campinas (Brazil) under the proposal XAFS1-15234 and by CEPROCOR, Córdoba (Argentina) under the regular budget of the Government of the Province of Córdoba / CEPROCOR 2014.

References

[1] S. Ackerman, R. Gieré, M. Newville, J. Majzlan, Antimony sinks in the weathering crust of bullets from Swiss shooting ranges, Sci. Total Environ. 407 (5) (2009) 1669–1682.
[2] C.A. Johnson, H. Moench, P. Wersin, P. Kugler, C. Wenger, Solubility of antimony and other elements in samples taken from shooting range, J. Environ. Qual. 34 (2005) 248–254.
[3] G. Cerriotti, D. Amarasiriwardena, A study of antimony complexed to soil-derived humic acids and inorganic antimony species along a Massachusetts highway, Microchem. J. 91 (2009) 85–93.
[4] W. Braida, C. Christodoulatos, A. Ogundipe, D. Dermatas, G. O'Connor, Electrokinetic treatment of firing ranges containing tungsten-contaminated soils, J. Hazard. Mater. 149 (2007) 562–567.
[5] M. Levonmaki, H. Hartikainen, T. Kairesalo, Effect of organic amendment and plant roots on the solubility and mobilization of lead in soils at a shooting range, J. Environ. Qual. 35 (4) (2006) 1026–1031.
[6] M. Chen, S.H. Daroub, L.Q. Ma, W.G. Harris, X. Cao, Characterization of lead in soils of a rifle/pistol shooting range in Central Florida, USA, Soil Sediment Contam. 11 (2002) 1–17.

[7] Z. Lin, B. Comet, U. Qvarfort, R. Herbert, The chemical and mineralogical behavior of Pb in shooting range soils from Central Sweden, Environ. Pollut. 89 (1995) 303–309.
[8] M. Rubio, A. Germanier, F. Mera, S.N. Faudone, R.D. Sbarato, J.M. Campos, V. Zampar, E. Bonzi, C.A. Pérez, Study of lead levels in soils by weathering of metallic Pb bullets used in dove hunting in Córdoba, Argentina, X-Ray Spectrom. 43 (2014) 186–192.
[9] I.X. Olivé, Mobility of lead and antimony in shooting range soils(Doctoral Thesis) ETH No. 16689, Swiss Federal Institute of Technology, Zurich, 2006.
[10] D. Vantelon, A. Lanzirotti, A.C. Scheinost, R. Kretzschmar, Spatial distribution and speciation of lead around corroding bullets in a shooting range soil studied by micro-X-ray fluorescence and absorption spectroscopy, Environ. Sci. Technol. 39 (2005) 4808–4815.
[11] A.C. Scheinost, A. Rossberg, D. Vantelon, I. Xifra, R. Kretzschmar, A. Leuz, H. Funke, C.A. Johnson, Quantitative antimony speciation in shooting-range soils by EXAFS spectroscopy, Geochim. Cosmochim. Acta 70 (2006) 3299–3312.
[12] S.S. Jorgensen, M. Willems, The fate of lead in soils: the transformation of lead pellets in shooting-range soils, Ambio 16 (1987) 11–15.
[13] G. Davies, E.A. Ghabbour, C. Steelink, Humic acids: marvelous products of soil chemistry, J. Chem. Educ. 78 (12) (2001) 1609–1614.
[14] B. Xing, Sorption of naphthalene and phenanthrene by soil humic acids, Environ. Pollut. 111 (2001) 303–309.
[15] L. Zhang, R. Hustache, O. Hignette, E. Ziegler, A. Freund, Design optimization of a flexural hinge-based bender for X-ray optics, J. Synchrotron Radiat. 5 (3) (1998) 804–807.
[16] V.A. Solé, E. Papillon, M. Cotte, Ph. Walter, J. Susini, A multiplatform code for the analysis of energy-dispersive X-ray fluorescence spectra, Spectrochim. Acta B 62 (2007) 63–68.
[17] C.A. Pérez, M. Radtke, H.J. Sanchez, H. Tolentino, R.T. Neuenshwander, W. Barg, M. Rubio, M.I.S. Bueno, I.M. Raimundo, J.J.R. Rohwedder, Synchrotron radiation X-ray fluorescence at the LNLS: beamline instrumentation and experiments, X-Ray Spectrom. 28 (1999) 320–326.
[18] R. Young, The Rietveld Method, International Union of Crystallography, Oxford University Press, Oxford, 1993.
[19] S. Enzo, W. Parish, A method of background subtraction for the analysis of broadened profiles, Adv. X-ray Anal. 27 (1983) 37–44.
[20] V. Galván Josa, S.R. Bertolino, A. Laguens, J.A. Riveros, G. Castellano, X-ray and scanning electron microscopy archaeometric studies of pigments from the Aguada culture, Argentina, Microchem. J. 96 (2010) 259–268.